Search for free decay of negative pions in water and light materials

T. Numao, Yu. I. Davydov, and J-M. Poutissou
TRIUMF, 4004 Wesbrook Mall, Vancouver, B.C., Canada V6T 2A3

T. C. Awes and V. Cianciolo
Oak Ridge National Laboratory, High Energy Physics, Oak Ridge, Tennessee 37831-6372, USA

S. Berridge, W. Bugg, Yu. Efremenko, R. Gearhart, and S. Ovchinnikov
University of Tennessee, Knoxville, Tennessee 37996-1200, USA
(Received 22 March 2006; published 26 May 2006)

We report on a search for the free-decay component of π^- stopped in water and light materials. A nonzero value of this would be an indication of anomalous $\bar{\nu}_e$ contamination to the ν_e and $\bar{\nu}_\mu$ production at stopped-pion neutrino facilities. No free-decay component of π^- was observed in water, Beryllium, and Aluminum, for which upper limits were established at 8.2×10^{-4}, 3.2×10^{-3}, and 7.7×10^{-3}, respectively.

DOI: 10.1103/PhysRevD.73.092004 PACS numbers: 14.60.Pq, 25.80.Hp, 29.25.−t, 36.10.−k

I. INTRODUCTION

Flavor suppression in the incident neutrino beam is one of the key elements for successful neutrino appearance experiments. In the case of beam-dump experiments using muon decays from stopped pions, the contribution to neutrino production from negative pions is expected to be significantly suppressed, because negative pions are believed to undergo nuclear capture promptly after stopping in material, while positive pions freely decay. The ratio of π^-/π^+ production cross sections for a proton beam in the 0.5–1 GeV energy region is about $1/5$ for light nuclei, which further enhances this asymmetry. The total neutrino content after the pion decay $\pi^+ \rightarrow \mu^+ \nu_\mu$ followed by the muon decay $\mu^+ \rightarrow e^+ \nu_e \bar{\nu}_\mu$ ($\pi^+ \rightarrow \mu^+ \rightarrow e^+$ decay) does not include $\bar{\nu}_e$'s in the final state. The contribution from decay-in-flight is a few percent for a pion. This provides a good opportunity for $\bar{\nu}_e$ appearance experiments [1–3]. However, a finite π^- lifetime in the stopping material may result in additional $\bar{\nu}_e$ contamination.

Normally, after stopping and being trapped in an atomic orbit, a negative pion orbiting the nucleus promptly deexcites by the Auger process, radiative cascade decays, or Stark mixing to an S state, where the significant overlap of the wave function with the nucleus enables the π^- to be captured by the nucleus. If the π^- is not captured by the nucleus it may decay freely in the atomic state. The free-decay fraction of π^-'s was measured to be 8.7×10^{-5} [4] in hydrogen and is expected to decrease with the atomic number. However, there is an exception in the π^- He atom system [5,6], where the π^- is trapped in a metastable state that has little wave function overlap with the nucleus and the Auger processes are suppressed [7]. It is therefore important to confirm the absence of other mechanisms that may cause free decays of π^-'s.

Limits for the fraction of the free-decay component exist for H_2 and He [4–6] (data in Ne is only applicable to a metastable state with a lifetime longer than ~1 ns). This paper reports the results of a search for a free-decay component of π^- in water and light materials from analyses of electron yields and proton spectra.

II. PRINCIPLE

Figure 1 illustrates the time diagrams involved in pionic-atom formation (left) up to the disappearance of the pion by (A) prompt nuclear capture, (b and B) free decay with a partial lifetime τ_π, and (C) delayed pion capture with a partial lifetime of τ_{capt}. The processes (a) and (c) feed into "π^- Atom" (right). Since the diagrams for delayed pionic-atom formation (left) and delayed nuclear capture (right) are identical, and since the two processes cannot be discriminated or separated in this analysis, the two processes are considered as a single process with prompt capture notation, i.e. R and τ_{capt} are used in this analysis. The

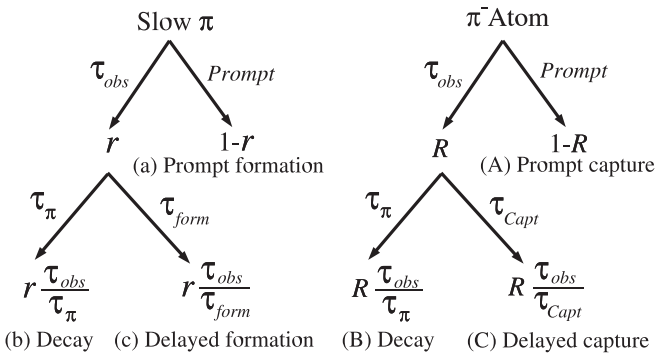

FIG. 1. Left: Pionic-atom formation processes, and Right: Atomic deexcitation and capture processes of the pionic atom. r and R are the fractions of delayed pionic-atom formation and delayed capture, respectively. τ_{form} and τ_{capt} indicate the partial lifetimes for delayed pionic-atom formation and delayed capture, respectively.

common observed lifetime, $\tau_{\rm obs} = 1/(\frac{1}{\tau_\pi} + \frac{1}{\tau_{\rm capt}})$, in the diagrams already assumes only delayed-capture process.

A direct method to search for free π^- decay is to detect decay products of pions (B). Detection of muons from the decay $\pi^- \rightarrow \mu^- \bar{\nu}$ in water is not practical because of the short muon range in water (~ 1.4 mm). However, electrons from the $\pi^- \rightarrow \mu^- \rightarrow e^-$ decay chain ($E_e =$ 0–53 MeV) can be detected. In this method, the background from decay-in-flight (DIF) of a pion to a muon, which stops in materials around the target and later decays to an electron, must be subtracted using Monte Carlo (MC) calculations. The advantages of the search for electrons from the decay $\pi^- \rightarrow \mu^- \rightarrow e^-$ are that the measurement is the sum of all free-decay components with different lifetimes and that the sensitivity does not strongly depend on the lifetime $\tau_{\rm obs}$; it varies only by $\sim$10% for the lifetime between 0 ns and the pion lifetime $\tau_\pi = 26.033$ ns [8].

Alternately, free π^- decay may be detected by the presence of electrons from the decay $\pi^- \rightarrow e^- \nu$. However, because of its small branching ratio, 1.231×10^{-4} [9], it is very difficult to differentiate it from the background arising from prompt nuclear capture γ-rays that convert in the target to an electron-positron pair. The search for $\pi^- \rightarrow e^- \bar{\nu}$ is effective for a component with a relatively long lifetime.

The third method (indirect) is to search for delayed components (C) in the time spectrum of pion capture products, such as protons, γ-rays, and π^0's. The ratio of delayed π^- capture $f_{\rm capt}$ is expressed as

$$f_{\rm capt} = \frac{\rm (C)}{\rm (A) + (C)} = \frac{R\frac{\tau_{\rm obs}}{\tau_{\rm capt}}}{1 - R + R\frac{\tau_{\rm obs}}{\tau_{\rm capt}}}. \qquad (1)$$

By eliminating R and $\tau_{\rm capt}$, which are not directly observable, the free-decay fraction (B) can be deduced,

$$\rm (B) = R \cdot \frac{\tau_{obs}}{\tau_\pi} = \frac{f_{capt} \cdot \tau_{obs}}{\tau_\pi - \tau_{obs} + f_{capt} \cdot \tau_{obs}}. \qquad (2)$$

It should be noted that when $\tau_{\rm obs}$ approaches τ_π the equation approaches to unity, indicating that the capture experiment is insensitive to the free-decay component as $\tau_{\rm capt}$ approaches infinity. In order to be sensitive to a fast decay component in the presence of the dominant prompt capture (the process (A)), the experiment is required to have good time resolution. In the search for delayed components in water, this can be achieved by measuring protons that have high energy losses, therefore, with small time walk and spread. Proton measurements are not sensitive to π^- capture by hydrogen in water, since only γ-rays, π^0's, and neutrons are produced. The majority ($> 99\%$) of π^-'s in water [10,11] are captured by oxygen atoms.

III. EXPERIMENT

The experiment was performed at the TRIUMF M9A channel. Typical ratios of incoming beam particles at the experimental target were $e{:}\mu{:}\pi = 5{:}1{:}4$ for a positive-particle beam and $e{:}\mu{:}\pi = 88{:}3{:}9$ for a negative-particle beam at $P_\pi = 70$ MeV/c with a momentum bite $\Delta P/P = \pm 4\%$. Figure 2 shows the detector setup. The position and the direction of incoming beam particles were measured by two sets of X-Y readout wire chambers (WC1 and WC2) located 95 cm and 50 cm upstream of the target. Two plastic scintillators B1 (76 mm high, 76 mm wide, 3.2 mm thick) and B2 (35 mm high, 25 mm wide, 5 mm thick) were placed 8 cm and 3 cm upstream of the target center, respectively. In order to collimate the beam (to detect scattered beam by e.g. the WC frames), a 305×305 mm^2 plastic counter with a 76 mm diameter hole (not shown in the figure) was placed 5 cm upstream of the B1 counter. Purified water for the target was held in a $60 \times 60 \times 8$ mm^3 container made of 0.2 mm thick aluminum frame and 50 μm thick beam windows (both ends). The target was tilted to 45 degrees with respect to the beam (some runs were taken at -45 degrees). A 152×152 mm^2 veto counter B3 for the detection of passing through beam particles was placed 40 cm downstream of the target. More than 90% of pions stopped in the target at a rate of 1–10 kHz for the π^- beam and 30–100 kHz for π^+.

The decay products were observed by two telescope arms at 5 cm from the beam axis at ± 90 degrees. Each telescope consisted of three 3–6 mm thick plastic scintillators (T1–T3 or M1–M3), and a 46 cm diameter, 51 cm long NaI(Tl) crystal (TINA) or a 36 cm diameter, 36 cm long NaI(Tl) (MINA). In each telescope, the farthest scintillator from the target was the largest one that covered the front face of the NaI for pileup detection. The solid angle of each telescope was defined by the 102×102 mm^2 T1 or the 76×76 mm^2 M1 counter. For π^0 detection, a 5 mm thick 51×51 mm^2 lead sheet was placed as a converter between the first and the second plastic scintillators in the MINA telescope.

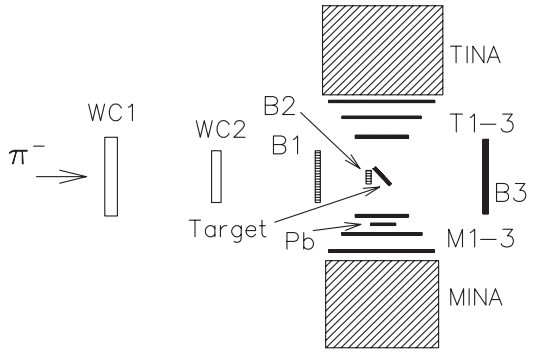

FIG. 2. Experimental setup. TINA and MINA are NaI(Tl) detectors described in the text.

The trigger required a pion stopping in the target (B1 · B2 · $\overline{B3}$) with the presence of an outgoing particle into the T2 or M2 counter in the time window from -50 ns to 150 ns with respect to the prompt time—this condition allowed to accept events containing electrons, γ-rays, π^0's (two γ-rays), protons, and deuterons. Typical trigger rates were 70 Hz for π^- runs and 150 Hz for π^+ with a deadtime of 10%–30%. The timing and pulse heights of all the scintillation counters, two coordinates from each wire chamber, and the relative phase of the 23.06 MHz cyclotron radio frequency (RF) (incident proton beam bunches) to the B2 counter time for the time-of-flight (TOF) measurement of a beam particle were recorded. In order to record pileup information, additional wide-gate (250 ns) analog-to-digital converters (ADC's) were employed using signals split from B1, B3, T3, and M3 counters for detection of extra charge outside the standard gate (50 ns). Pileup in the NaI counters was measured by using two additional ADC's with an early gate that closed just before the main pulse, and a late gate (by 200 ns) to compare to the normal gate ADC.

Special runs were taken for calibration and normalization; runs with a trigger using a pulser driven by a prescaled cyclotron RF signal, runs requiring only the presence of incoming particles (B1 · B2), and runs with positive beam particles (for normalization of the electron acceptance). For $\pi \to \mu \to e$ measurement, a 30 mm diameter, 12 mm thick cylindrical water target was used without tilting, together with a 25 mm diameter, 5 mm thick B2 counter that faced the target with a variable gap between $z = 0$–3.5 cm. Also, other candidate materials for the beam moderators at a neutrino factory, beryllium ($50 \times 50 \times 8$ mm^3) and aluminum ($75 \times 75 \times 6$ mm^3), were used as targets during several runs. A vinegar target (5% acetic acid by volume) was used to simulate possible effects of excessive H^+ ions in water generated by the high-intensity proton beam of the stopped-beam facility. Measurement was made at beam momenta of 64, 67, 70, 73, 76, and 80 MeV/c to confirm the stopping position of pions and to test systematic effects.

IV. ANALYSIS

Beam pions were identified by the energy loss in the first beam counter B1, and the TOF with respect to the proton beam bunch. Figure 3 shows a scatter plot of B1 counter energy vs RF time with respect to the B2 time after the time walk correction. At the experimental target position (about 10 m from the pion production target), the TOF of electrons coming from the next beam bucket was separated from that of 70 MeV/c pions, and the probability of misidentifying a beam electron as a pion was estimated to be $\sim 2 \times 10^{-7}$. The TOF peak of muons was clearly separated.

The beam counters were calibrated using estimated energy losses of e's, μ's, and π's that passed through the

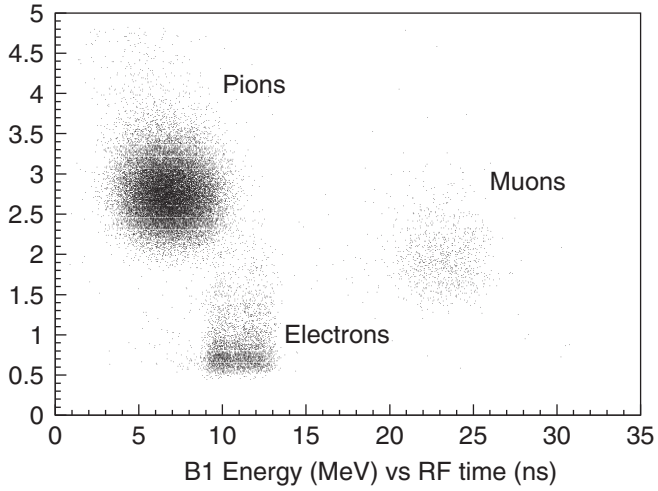

FIG. 3. Energy in B1 vs beam burst (RF) time with respect to B2 time. The time walk effect in the B2 counter has been corrected.

counters. The telescope counters were calibrated with positrons from $\mu^+ \to e^+ \nu \bar{\nu}$ decays, $\pi^+ \to e^+ \nu$ decays, and scattered beam particles. For TINA and MINA, energy losses in the telescope counters and the 1 MeV shift due to positron annihilation were taken into account. Time calibration was based on the repeated peaks with the RF cycle in the time spectra. Figure 4 shows a scatter plot of energy in the T2 counter vs energy in TINA, in which the diagonal band is from protons produced by pion capture, the flat distribution around the energy loss of 2 MeV/cm is from electrons (up to 45 MeV from $\mu \to e \nu \bar{\nu}$ decays and around 60 MeV from scattered beam electrons), and the distribu-

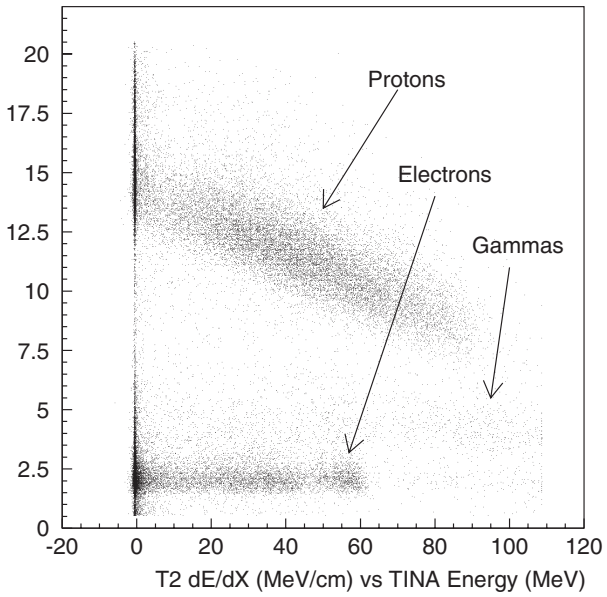

FIG. 4. Energy loss in T2 (MeV/cm) vs energy in TINA (MeV). Electrons below 45 MeV are from $\pi \to \mu \to e$ decays and around 60 MeV are from electron scattering.

tion around 100 MeV with twice the energy loss of electrons in the T2 counter is from electron-positron pairs from γ-rays converted in the T1 counter or the target.

A. Analysis of $\pi \to \mu \to e$ decay

In the analysis of $\pi^- \to \mu^- \to e^-$ decay events, data taken with the circular water target were used. Pulse heights in the three telescope counters T1–T3 were required to be less than $\sim$7 MeV/cm. The effect of the loss by this cut ($\sim 3\%$) cancelled when the yield was normalized to that of $\pi^+ \to \mu^+ \to e^+$. No proton contamination below $E = 80$ MeV was observed. Some events from two ''electrons'' were accepted with the dE/dx cut in the T-counters, but they appeared together with scattered beam electrons at the prompt time and at every 43 ns with respect to the prompt time. Only delayed events outside those affected regions ($t_e = 48$–81 ns with respect to the prompt time t_0)[12] were selected for the analysis.

The histogram of Fig. 5 shows the energy spectrum measured in the B2 counter for the events that passed the above cuts. The position of the B2 counter was in contact with the target ($z = 0$ cm). DIF contributions before and after passing the B2 counter are the major remaining components. Events from decays after passing the B2 counter form a peak around 5 MeV that corresponds to energy loss of pions passing through the B2 counter prior to stopping in the target. Events from the decays before passing the B2 counter form a broad distribution with a shoulder around 3.5 MeV that corresponds to the energy loss of the highest energy muons (~ 32 MeV for forward pion decays) and the lower energy events are from the backward-decay muons that stopped in the B2 counter.

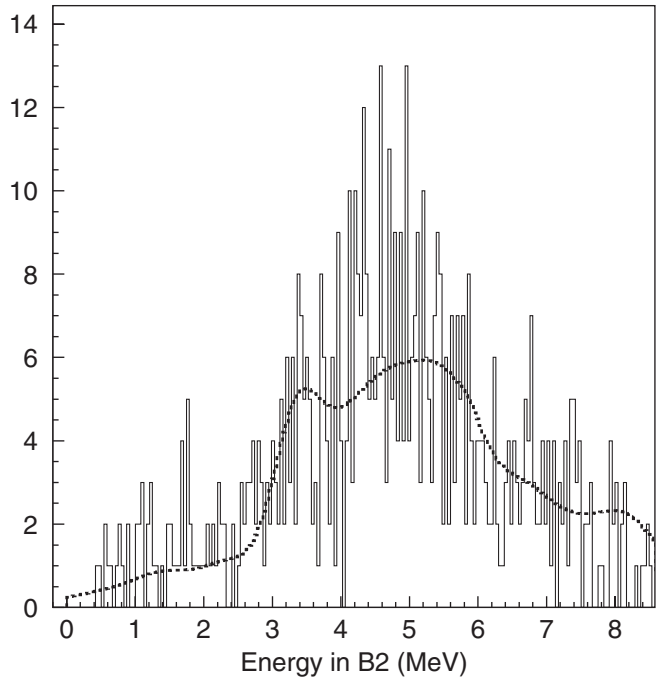

FIG. 5. Energy spectrum measured in the B2 counter. The dotted line shows the result of MC calculation normalized to the total count in the spectrum.

The contribution of DIF events was simulated by MC based on GEANT3 [13] with a modification for the π^- treatment. Pions were generated at the exit of the beam pipe (110 cm upstream of the target) with a profile of 10×10 cm^2 projecting to the target (2×2 cm^2) according to a flat momentum distribution centered at 70($\pm$4%) MeV/c that reproduced the measured energy spectrum of pions taken with a beam trigger. When a π^- stopped in material, it was promptly captured (capture products were not generated in the $\pi \to \mu \to e$ simulation). Muon capture was not included in the MC, but the effect was included in the lifetime correction by using the free muon lifetime instead of the lifetime of the muonic atom [14]. The effect of the binding energy (0.2 MeV for the muonic oxygen atom) on the electron spectrum was ignored. The MC events were analyzed with the same selection criteria as the experimental data and the energy spectrum in the B2 counter was obtained as shown by the dotted line in Fig. 5 (normalized to the total count). The shape of the distribution is well reproduced by MC calculations of the DIF events described above. The ratio of the two components in the MC spectrum, the peak (DIF after B2), and the broad bump (DIF before B2), strongly depended on the gap z, especially near the target ($z = 0$ cm). Although the peak is, in principle, more sensitive to the free-decay component, the sum was used in the analysis because of this strong dependence near $z = 0$ cm for reliable subtraction of the background estimated by the MC calculations. The contamination from the μ's in the beam was negligible.

In order to obtain the free-decay component fraction, the yield was normalized to that of the $\pi^+ \to \mu^+ \to e^+$ decays in the same time window with the corrections for the lifetime and the stopping fractions obtained from the beam-trigger data (f_{π^+}:$f_{\pi^-} = 0.81$:0.69) [15]. The second column in Table I shows the gap dependence of the free-decay fractions, which are dominated by the DIF contribution. For the normalization of the MC calculations, π^+ data were also generated and analyzed in the same way.

TABLE I. Summary of $\pi \to \mu \to e$ analysis for the water target. To obtain the free-decay fractions for the experimental data and the MC calculations, the yields have been normalized to those from π^+, and the time-window correction has been applied.

Gap (cm)	Free-decay fractions	
	Measured (%)	MC (%)
0	1.12 $\pm$ 0.04	1.09 $\pm$ 0.03
	1.09 $\pm$ 0.04	
1.4	1.26 $\pm$ 0.05	1.17 $\pm$ 0.04
3.5	1.15 $\pm$ 0.04	1.07 $\pm$ 0.03

The last column in Table I summarizes the corresponding fractions from the MC calculations.

The two measurements at $z = 0$ cm represent data with a possible beam position shift due to the magnet setup adjustment to correct for the hysteresis effect. The average of two measurements at $z = 0$ cm was used as the final result. An upper limit based on Bayesian method assuming a Gaussian probability distribution was obtained by subtracting the MC result and adding the associated errors in quadrature, and then renormalizing the area above zero. The obtained 90% confidence level (C.L.) upper limit of the $\pi \to \mu \to e$ amplitude corresponds to free-decay fraction of 7.5×10^{-4} for a short lifetime and 8.2×10^{-4} for a lifetime of the free-decay component near $\tau_{\rm obs} = \tau_\pi$.

B. Analysis of $\pi \to e\nu$ decay

The signal region was defined by a box cut of $t_e =$ 5–100 ns and $E_e = 60$–72 MeV in TINA. Event selection criteria for the $\pi \to e\nu$ decay analysis were tighter than those used in the $\pi \to \mu \to e$ analysis because of its small branching ratio and sensitivity to background. A typical type of background occurred when a pion stopped in the target and an additional beam electron was scattered into TINA. Protection against this came from efficient beam pileup detection and the high TINA energy threshold—the presence of extra beam particles during the search time window was detected by tighter energy loss cuts in the B1 and B2 counters as well as by comparing the pulse charges observed in the narrow-gate and wide-gate ADC's for the B1 counter. Using the observed pileup data and beam

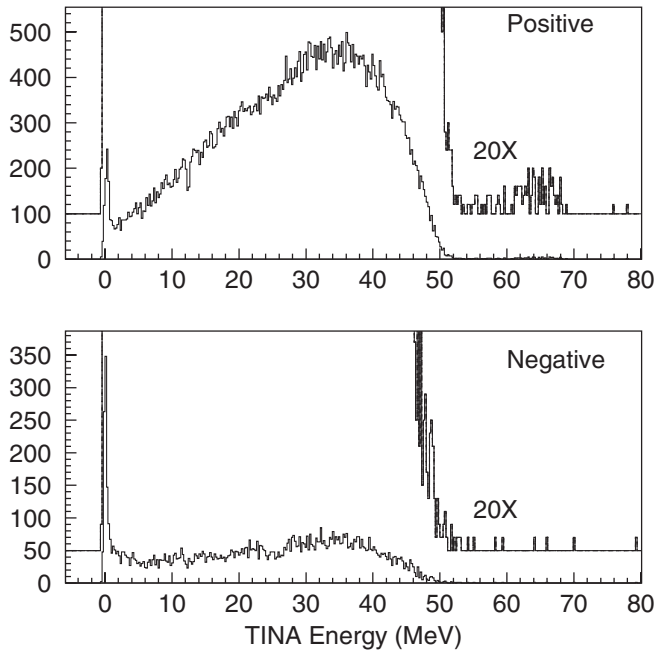

FIG. 6. Energy spectra in TINA for π^+ (top) and π^- (bottom) stopping in H_2O. Events in the energy region of 60–70 MeV are mainly from $\pi \to e\nu$ decays.

TABLE II. Summary of $\pi \to e\nu$ analysis. The 90% C.L. upper limits of the free-decay fractions are shown in the last column for the case when $\tau_{\rm obs} = \tau_\pi$.

	π^-		π^+		Free-decay
Material	$\pi \to e\nu$	π stops	$\pi \to e\nu$	π stops	90% C.L.
H_2O	3	1.29×10^9	69	5.23×10^7	4.6×10^{-3}
Be	1	8.32×10^8	94	5.40×10^7	3.1×10^{-3}
Al	1	3.34×10^8	114	6.38×10^7	7.6×10^{-3}
Vinegar	0	4.51×10^8	69	5.23×10^7	4.5×10^{-3}

electron energy spectra, the level of this background in terms of free-decay fraction was estimated to be 4×10^{-3}. Pileup in TINA that shifts the energy of $\pi \to \mu \to e$ events into the signal region was another concern. Early pileup in TINA was detected by the ADC with an early gate that closed at the beginning of the normal signal. Other pileup was detected by a set of two ADC's with different gate widths for TINA and T3. This background was $<1\%$ of $\pi^+ \to e^+\nu$ decays and significantly suppressed for π^- by the lack of free pion decays.

Figure 6 shows energy spectra in TINA for π^+ (top) and π^- (bottom) runs with the water target. Some events were seen in the time-energy box with time distribution consistent with the electron scattering background, though they were included in the free-decay candidates. 90% C.L. upper limits were obtained assuming Poisson statistics with no background. The limits were normalized to the corresponding π^+ data with the time-window corrections. The results are summarized in Table II. The 90% C.L. limits shown in the table correspond to the case when the free-decay component has the pion lifetime. These limits are complementary to the capture measurements.

C. Analysis of capture products

In the search for free π^- decay via detection of delayed protons from π^- capture, good timing is essential to be sensitive to fast decay components. In order to minimize the time smearing, the energy loss as well as the TOF cuts in the selection of pions (typically $\pm 3\sigma$ away from the peak) were tighter than those used in the electron analysis. Selection of protons was made based on the energy loss in all the three T counters; the threshold for each counter was set around 4 times that of minimum ionizing particles. The resulting cutoff energy for accepted protons was around 45 MeV in the incident energy. The contributions from electron and muon contaminations in the beam were negligible.

Without corrections the time resolution of the prompt peak was $\sigma \sim 1$ ns. There were many effects that caused timing shift and spread; (1) the beam momentum distribution that affected the energy loss in the beam counters, the horizontal stopping position, and the TOF, (2) the pulse height dependences (time walk) in the beam counters and

telescope counters, which were correlated with the energy loss and the proton emission angle, (3) the path length variation, e.g. due to the pion stopping position and the emission angle of protons, and (4) the propagation time of the light in the scintillator especially in telescope counters T1, T2, and T3. Many effects were correlated with one another. Correction factors were obtained by minimizing the dependence of the t_0 on each measured parameter, such as pulse heights, timing in the beam counters and telescope counters, and horizontal pion stopping positions. A linear dependence was used to obtain corrections. New correction factors were calculated at the end of each iteration and the revised correction factors were applied in the next iteration (only half of the amount was corrected each time). The process converged after about ten iterations. The corrections improved the timing resolution to $\sigma \sim 200$ ps. These corrections do not affect the amount of the real decay component since the free-decay component fraction is independent of the parameters used in the optimization.

Figure 7 shows time spectra for H_2O, beryllium, aluminum, and vinegar. The time spectra of protons for all targets show essentially a single component, a Gaussian peak at t_0, as indicated by the solid line for a single Gaussian fit with three parameters; the amplitude, offset, and width, reflecting the resolution. In the data from early stage of the experiment, there was an obvious delayed component, a bump at $t_p = 1$–2 ns that was enhanced when the events stopping in the upper half of the target were selected. The appearance of the delayed component coincided with the runs with the water target filled only up to 85% of the height. These suggested some slow pions stopped outside the target (probably downstream of the target) with a longer flight path for the resulting proton. MC calculations indicated that, when the target was lowered by the half height of the beam, about 0.3% pions stopped on the surface of the material around the telescope counters and had a similar time distribution. Since the extra counts outside the Gaussian distribution could not positively be identified as background, we treated them as a potential signal and only upper limits are quoted.

For the extraction of a possible delayed component by the time spectrum fit, the function used in the fit was a Gaussian plus an exponential function including the resolution effect (the same resolution was used). Assuming only one decay constant for the delayed component, a likelihood function Lk

$$Lk = \prod_{i=1}^{n} \frac{N_i^{n_i} e^{-N_i}}{n_i!} \Big/ \prod_{i=1}^{n} \frac{n_i^{n_i} e^{-n_i}}{n_i!}, \tag{3}$$

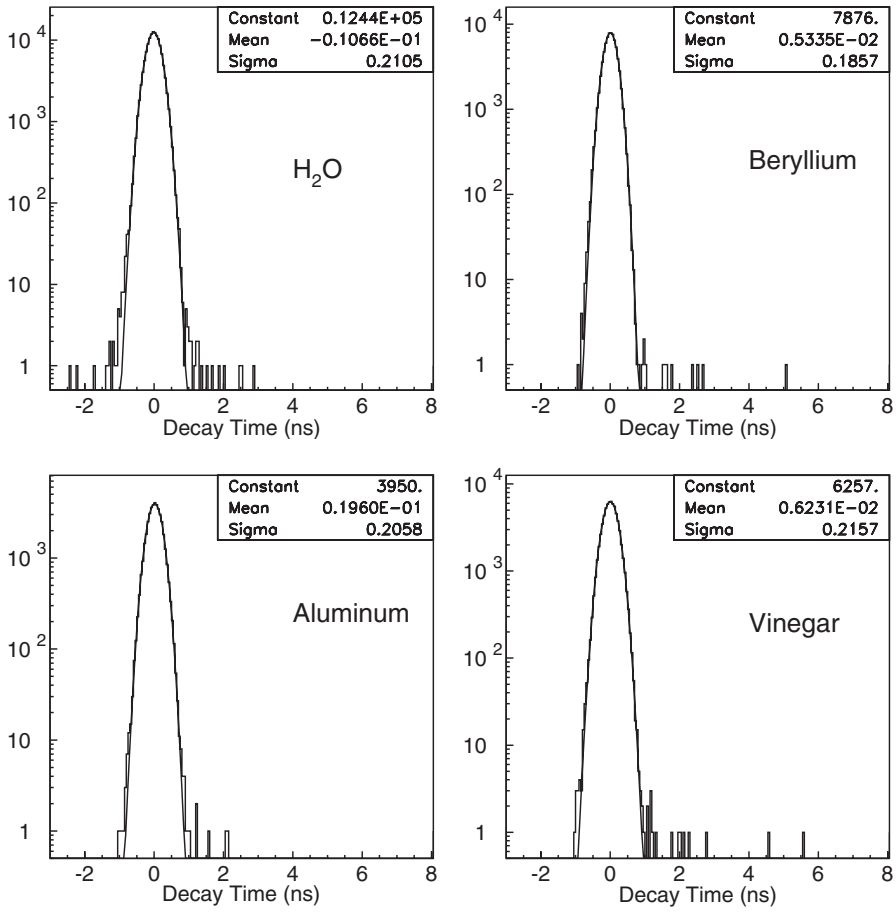

FIG. 7. Time spectra of protons for H_2O, Be, Al, and vinegar (histograms). The solid curves show Gaussian fits.

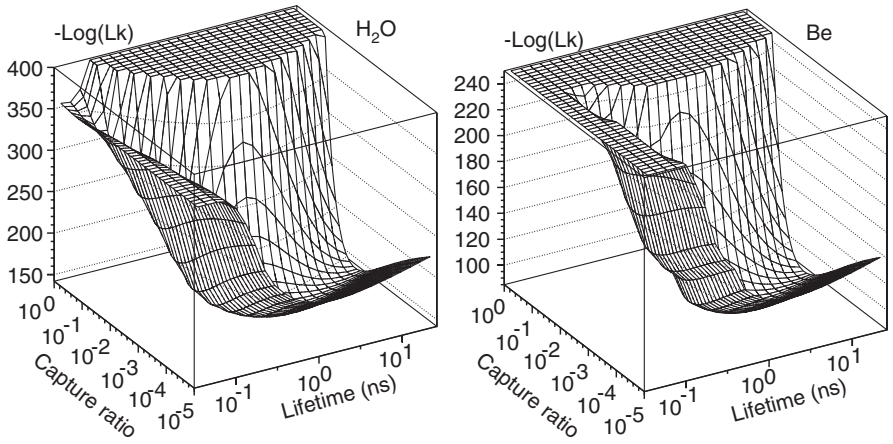

FIG. 8. $-\log(Lk)$ for H_2O and beryllium. Large $-\log Lk$ values were truncated for display.

where n_i and N_i are the data and fitted value for the ith bin, respectively, was maximized with three variable parameters; the total counts, the resolution, and the t_0, but the lifetime and the capture ratio of the delayed component were fixed for each maximization process, and the minimum in $-\log Lk$ was stored for each set of lifetime and delayed-capture ratio. Figure 8 shows surface plots of the likelihood functions $-\log Lk$ for the delayed-capture ratio and the lifetime. The dotted histograms in Fig. 9 show the 90% C.L. upper limits of the delayed-capture ratio f_{capt} for each lifetime.

In order to test the validity of using a single Gaussian distribution for the prompt capture timing peak, a possible asymmetric time distribution, due to e.g. solid angle effects causing different weight for different TOF, was simulated by MC. Capture products were generated as soon as they stopped; pion capture-in-flight was simulated separately. Proton and deuteron spectra were taken from Ref. [16] and interpolated in energy and atomic number. Other heavier particles were ignored because of higher stopping power that prevented them from contributing to a trigger. The MC events were calibrated in the same way as the experimental data to reflect the effects of the corrections in timing spectrum, and analyzed with the same program with the same cuts. After smearing with a resolution of 200 ps (the bare resolution of MC was about 60 ps after applying corrections), the spectrum was fitted to a Gaussian curve. The fit agreed at the 10^{-4}–10^{-5} level, and the asymmetry was not significant.

The effect of capture-in-flight was simulated with the total cross section [17], $\sigma_{\text{total}} = \pi r_0^2 \cdot (1 + \frac{E_C}{T_\pi})$, where $r_0 = 1.25 \cdot A^{1/3}$ (fm) is the nuclear radius, and $E_C = 1.44 \cdot Z/r_0$ (MeV) is the Coulomb potential. A and Z are the mass and atomic numbers of the target material (hydrogen was ignored for scintillator and water), respectively. The nuclear absorption cross section was assumed to be $1/3$ of the total cross section, and the capture products were generated by ignoring the kinetic energy of the pion. Inclusion of the capture-in-flight process increased the number of events in the early time region ($t_p = -0.5$ ns)

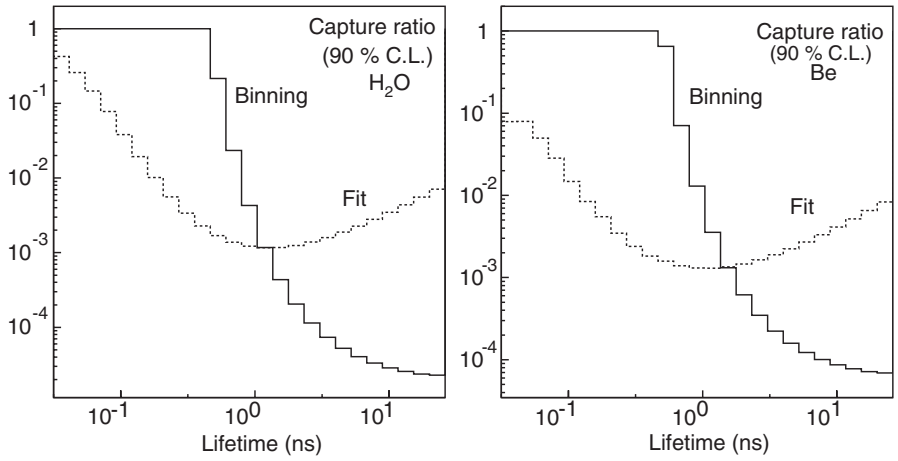

FIG. 9. 90% C.L. upper limits of delayed-capture ratios f_{capt} for H_2O and beryllium as a function of assumed lifetime. The true 90% C.L. limits around the 1 ns region may lie along a curve that smoothly connects the binning and fit results.

TABLE III. Summary of binning analysis of proton data. The second column shows the numbers of candidate events in the time bin 5–75 ns. The 90% C.L. upper limits for delayed-capture ratios in the last column are for $\tau_{\rm obs} = \tau_\pi$ with the corresponding time-window correction of 0.769.

Material	Candidates	Total events	90% C.L. ratios
H_2O	0	1.31×10^5	2.3×10^{-5}
Be	1	7.35×10^4	6.9×10^{-5}
Al	0	4.08×10^4	7.3×10^{-5}
Vinegar	1	6.77×10^4	7.5×10^{-5}

by 0.1% of the total counts, which was consistent with the excess counts in the same time region of the data. However, the capture ratio of the delayed component was unaffected by this.

In the long lifetime region, the fit results were affected by the small sample bias of the maximum likelihood method. A simple time bin method was employed for this region; events in the time bin of $t_p = 5$–75 ns were considered to be possible candidates, and the sum in the time bin was normalized to the total number of events in the proton spectrum. A Poisson distribution was assumed to obtain the 90% C.L. upper limit. Table III summarizes the results for H_2O, Be, Al, and vinegar. The solid lines in Fig. 9 show the results from the binning method.

The observed delayed-capture ratio was converted to the fraction of free π^- decay using Eq. (2). The summary of the proton analysis is shown in Fig. 10, where the dashed lines indicate the 90% C.L. limits for the free-decay component obtained by the fits, and the solid lines by the binning method. The capture limits go to unity at the pion lifetime (the next bin outside the spectrum). In the shorter lifetime region outside the plot, the upper limit is along the extension of the binning result, which corresponds to $\tau_{\rm obs}/\tau_\pi$. The results from the $\pi \to \mu \to e$ (dash-dotted line) and $\pi \to e\nu$ (dotted line) analyses are also shown in the figure. Without knowing the lifetime of the delayed component, conservative limits obtained near the pion lifetime (the largest upper limits) for all cases are: 8.2×10^{-4} for H_2O by the $\pi \to \mu \to e$ analysis at $\tau_{\rm obs} = \tau_\pi$, and 3.2×10^{-3} for beryllium, 7.7×10^{-3} for alumi-

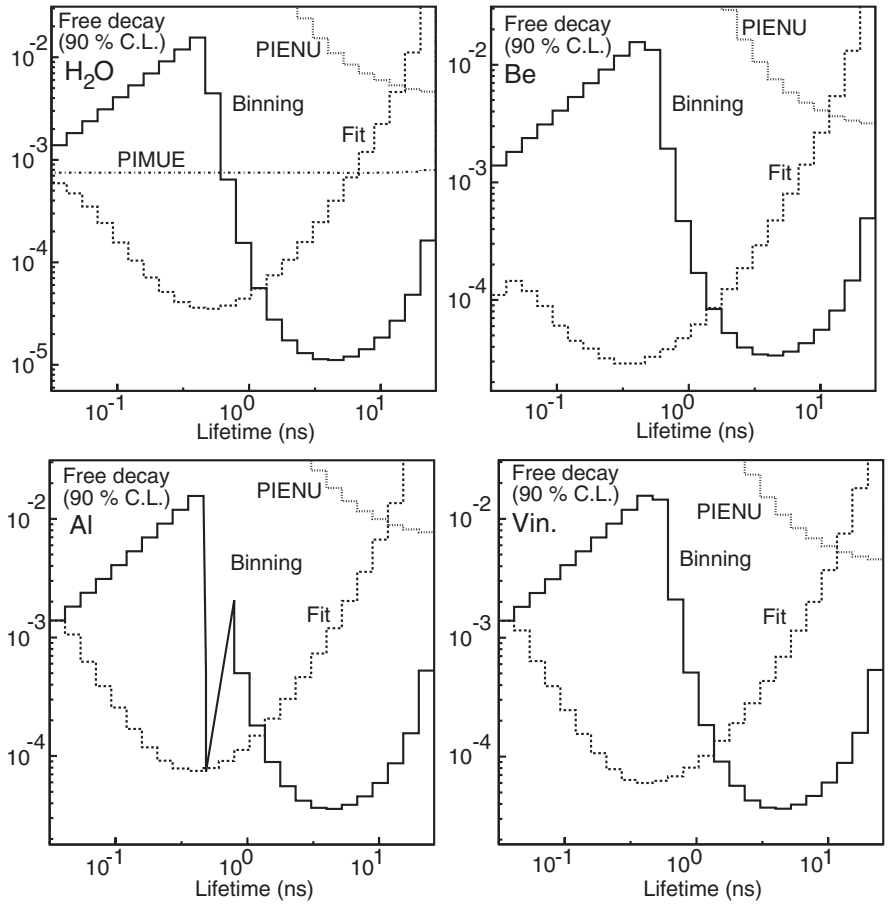

FIG. 10. 90% C.L. upper limits of free-decay fractions for H_2O, Be, Al, and vinegar. The dashed histograms are the results by fit, the solid histograms by binning for the delayed-capture method, the dotted histograms by $\pi \to e\nu$, and the dash-dotted line by $\pi \to \mu \to e$.

num, and 4.5×10^{-3} for vinegar by $\pi \rightarrow e\nu$ at the intersection of the binning and $\pi \rightarrow e\nu$ limits.

V. CONCLUSION

No free π^--decay component was observed in water with the "90% C.L." upper limit for the free-decay fraction of 8.2×10^{-4} for the worst case ($\tau_{\rm obs} = \tau_\pi$). For beryllium and aluminum assuming a single delayed component, the limits were 3.2×10^{-3} and 7.7×10^{-3} coming from the measurements of $\pi^- \rightarrow e^- \bar{\nu}$ decays, respectively. The result of the present experiment indicates that the materials studied here will not cause $\bar{\nu}_e$ contamination in the beam-dump neutrino experiments. It seems unlikely that the LSND result [1], which would require the relative $\bar{\nu}_e$ yield of $>10^{-2}$ [18], can be explained by the mechanism of unusual formation or deexcitation processes of pionic atoms in water.

ACKNOWLEDGMENTS

The authors would like to express their gratitude to P. Amaudruz for his help in setting up the data acquisition system. This work was in part supported by the National Council of Canada, the National Science Foundation, and the Devision of Nuclear Physics, Department of Energy.

[1] C. Athanassopoulos *et al.*, Phys. Rev. C **54**, 2685 (1996).
[2] B. Armbruster *et al.*, Phys. Rev. D **65**, 112001 (2002).
[3] F. T. Avignone and Yu. Efremenko, J. Phys. G **29**, 2665 (2003).
[4] T. H. Fields *et al.*, Phys. Rev. Lett. **5**, 69 (1960); J. H. Doede *et al.*, Phys. Rev. **129**, 2808 (1963).
[5] J. G. Fetkovich and E. G. Pewitt, Phys. Rev. Lett. **11**, 290 (1963); M. M. Block *et al.*, Phys. Rev. Lett. **11**, 301 (1963).
[6] S. N. Nakamura *et al.*, Phys. Rev. A **45**, 6202 (1992).
[7] G. T. Condo, Phys. Lett. **9**, 65 (1964); I. Shimamura, Phys. Rev. A **46**, 3776 (1992), and references therein.
[8] T. Numao, J. A. Macdonald, G. M. Marshall, A. Olin, and M. C. Fujiwara, Phys. Rev. D **52**, 4855 (1995); V. P. Koptev *et al.*, Zh. Eksp. Teor. Fiz. **61**, 865 (1995) [JETP Lett. **61**, 877 (1995)].
[9] D. I. Britton *et al.*, Phys. Rev. Lett. **68**, 3000 (1992); G. Czapek *et al.*, Phys. Rev. Lett. **70**, 17 (1993).
[10] A. F. Dunaitsev *et al.*, Nuovo Cimento **34**, 5569 (1964).
[11] Z. V. Krumshtein *et al.*, Sov. Phys. JETP **27**, 906 (1968).
[12] The corresponding early time region $t_e = 5$–38 ns suffers from the tail of prompt events. It is also less sensitive to slow decay components.
[13] R. Brun *et al.*, GEANT3 Detector Description and Simulation Tool Reference Manual (1994).
[14] For the early μ-decay time window between t_1 and t_2, the product of the muon-decay fraction τ_A/τ_μ and the time acceptance $e^{-t_1/\tau_A} - e^{-t_2/\tau_A}$ can be approximated to $e^{-t_1/\tau_\mu} - e^{-t_2/\tau_\mu}$, where τ_A is the lifetime of the muonic atom. The advantage of this approach over the use of muonic atom is that the contributions from μ-decays in different materials can be added with a single lifetime.
[15] The online definition of "stop" ($B1 \cdot B2 \cdot \overline{B3}$) allowed contributions from positrons (10%) and electrons (30%–40%).
[16] H. S. Pruys *et al.*, Nucl. Phys. **A352**, 388 (1981); F. W. Schleputz, J. C. Comiso, T. C. Meyer, and K. O. H. Ziock, Phys. Rev. C **19**, 135 (1979); G. Mechtersheimer *et al.*, Nucl. Phys. **A324**, 379 (1979).
[17] The expression simulates low energy behavior due to the Coulomb attraction. See, R. M. Sternheimer, Phys. Rev. **101**, 384 (1956).
[18] The signal to $\bar{\nu}_e$-originated background ratio was $\sim$15 with the expected $\bar{\nu}_e/\bar{\nu}_\mu$ flux ratio of 7.8×10^{-4}. Considering the π^+/π^- production ratio and the pion stopping ratio in the water target, the required free-decay fraction to explain the LSND result could be as high as 0.1–1.